Materials Advances

ROYAL SOCIETY OF CHEMISTRY

PAPER

View Article Online
View Journal | View Issue

Cite this: *Mater. Adv.*, 2023, 4, 5785

Exploring 2D hexagonal WO_3/COK-12 nanostructures for efficient humidity detection

Bhavna Rohilla, [a] Aryan Boora,[a] M. S. Goyat [b] and Surender Duhan *[a]

This research reports a pioneering approach to humidity sensing by leveraging the unique properties of 2D hexagonal mesoporous COK-12 (Centrum voor Oppervlaktechemie & Katalyse-12/Center for Surface Chemistry & Catalysis – 12). In this research, the utilization of these innovative COK-12 structures showcases their potential for advancing humidity-sensing technology, marking a significant stride in the field of surface chemistry and catalysis. We investigated how electrical resistance changes in (x-WO_3)/COK-12 (with x = 0%, 1%, 3%, 6%, and 9%) with varying humidity levels. The samples containing diverse tungsten concentrations in COK-12 were synthesized by a hydrothermal method and characterized using appropriate tools. The results demonstrate the successful integration of tungsten ions into COK-12, maintaining its distinctive hexagonal mesoporous structure and high specific surface area (864 m^2 g^{-1}). Tungsten-doped COK-12 humidity sensors exhibit great sensitivity and response speed due to modified conductivity under humid conditions, enhancing moisture measurement precision. Notably, the 6%-WO_3/COK-12 sensor exhibits a linear correlation between relative humidity and electrical resistance, signifying strong sensitivity. The sensor displays a significant 4.3 orders of magnitude resistance shift, with rapid 12 s response and 11 s recovery times. These findings enhance our understanding of COK-12's humidity sensing capabilities, opening avenues for diverse applications like environmental monitoring, weather forecasting, and industrial processes including catalysis, adsorption, and drug delivery.

Received 10th September 2023,
Accepted 23rd October 2023

DOI: 10.1039/d3ma00691c

rsc.li/materials-advances

1. Introduction

Humidity sensing is fundamental in various fields from meteorology and agriculture to electronics and healthcare. Precise and reliable humidity measurements are crucial for maintaining optimal conditions, ensuring product quality, and understanding environmental dynamics.[1] For instance, consider semiconductor manufacturing where it is essential to uphold very low moisture levels. Higher levels can disrupt equipment efficiency, leading to a reduced quality and yield of semiconductor devices. Consequently, prior to commencing experimental procedures, it becomes essential to gauge the moisture content present in the operational environment to preempt any influence on the experimental outcomes. Significantly, the term "humidity" commonly denotes the volume of water vapor within the atmosphere.[2,3]

Humidity detection plays a crucial role in numerous industries, but it is not without its share of challenges. Achieving high sensitivity, especially in low-humidity environments, is a primary hurdle. Ensuring fast response times and maintaining accuracy across a wide range of humidity levels are also essential requirements.[4,5] To tackle these challenges, researchers have explored various methodologies. Capacitive sensors, which gauge changes in capacitance as humidity fluctuates, offer both high sensitivity and rapid response times.[6] Resistive sensors, which alter resistance in response to humidity, provide cost-effective alternatives. Optical sensors, capable of measuring changes in light transmission or reflection due to humidity variations, excel in accuracy.[7] Micro-electro-mechanical systems (MEMS) technology remains a pivotal area, with a focus on improving accuracy and reliability. Two-dimensional materials like graphene have garnered interest for their remarkable sensitivity to humidity changes and applications in wearables. Nanotechnology and nanomaterials have been harnessed to enhance sensor performance.[8] Wireless connectivity and integration into the Internet of Things (IoT) have gained momentum for real-time monitoring. Energy-efficient, calibrated, and flexible sensors are under development. Machine learning integration and applications in environmental monitoring, particularly in agriculture and weather forecasting, are also being explored.[6–8] Self-powered voltage humidity sensors harness energy from the environment, such as moisture or temperature differentials, to generate the voltage required for humidity measurements. This innovative approach eliminates the need for external power

[a] *Advanced Sensors Lab, Department of Physics, Deenbandhu Chhotu Ram University of Science and Technology, Murthal, Sonipat-131039, Haryana, India. E-mail: surender6561@gmail.com*
[b] *Department of Applied Science, School of Engineering, University of Petroleum and Energy Studies, Dehradun, 248007, Uttarakhand, India*

sources, making them highly suitable for remote and low-power applications like IoT devices, ensuring sustainability and efficiency.[9,10]

The field of humidity detection has been significantly transformed by the integration of nano-materials. They exist in various forms, including nanoparticles, nanowires, nanofilms, and nanocomposites, each offering unique benefits.[4] The choice of nanomaterials for humidity sensors should align with specific application requirements, considering sensitivity, response time, stability, and cost. Ongoing research in nanomaterials continues to enhance humidity sensor performance.[6] Metal oxide nanomaterials like titanium dioxide (TiO_2), zinc oxide (ZnO), and tungsten oxide (WO_3) are cost-effective and sensitive but may have slower response times. Carbon-based nanomaterials like carbon nanotubes (CNTs) and graphene offer exceptional sensitivity and rapid response.[11] Nanocomposites combine various nanomaterials, heightening sensitivity and response. 2-D materials like molybdenum disulfide (MoS_2) show promise due to their high surface-to-volume ratio. Nanowires, nanorods, metal–organic frameworks (MOFs), and polymer nanocomposites also contribute to improved humidity sensing.

Nonetheless, nano-based humidity sensing faces its own set of challenges. Some materials may lack stability or prove sensitive to environmental conditions, raising concerns about reliability.[4,11] Furthermore, the production costs associated with nano-materials can be prohibitive, potentially limiting widespread adoption. The integration of these materials into sensor devices may also pose technical challenges, necessitating careful engineering solutions.[12]

COK-12 is an innovative humidity sensor material that belongs to the family of ordered mesoporous silica (OMS) materials, like Santa Barbara Amorphous-15 (SBA-15). It is characterized by its hexagonally-packed cylindrical ordered pores, which have a diameter of 5.5–6 nm. One of the major advantages of COK-12 is that it can be synthesized at room temperature under mild reaction conditions, making it more time-efficient, cost-effective, and environmentally friendly compared to other OMS materials.[13,14] Its unique properties make it an ideal candidate for various applications, including humidity sensing. Tungsten oxide (WO_3) has a high melting point, excellent electrochromic properties, good catalytic activity, and good electrical conductivity. In addition, it is a hygroscopic material, which means it has the ability to absorb moisture from the surrounding environment.[15] This property makes it an excellent candidate for use in humidity sensors. When tungsten oxide absorbs moisture, it undergoes a change in its electrical conductivity, making it a sensitive indicator of humidity levels.[16] The extent of this change in conductivity is dependent on the level of humidity present, which allows for accurate measurement and monitoring of humidity levels.[17] The tungsten doping improves the sensor's sensitivity and stability by reducing its response time. The tungsten-doped COK-12 sensor can withstand temperatures of up to 150 °C and is suitable for use in industrial settings, such as power plants and factories.[18] Overall, the WO_3/COK-12 humidity sensor is a reliable and effective solution for measuring humidity in various applications.[19,20] In addition, the surface of COK-12 can be functionalized with various organic and inorganic molecules to enhance its sensing properties. This enables the sensor to selectively detect specific gases or vapors in complex gas mixtures.

In this study, we successfully developed a humidity sensor of remarkable sensitivity utilizing WO_3/COK-12 as a sensing material, featuring an intricately ordered 2D hexagonal architecture. The sensor design incorporates a layer of the synthesized material onto Ag–Pd interdigitated electrodes, while controlled conditions were established using sealed containers containing saturated salt solutions to emulate various environmental humidity levels. Additionally, we put forth a novel theoretical model grounded in the Grotthuss mechanism, elucidating the underlying humidity sensing principles at play within the WO_3/COK-12 sensor. Furthermore, the crafted nanostructures exhibit impressively organized mesoporous architectures characterized by unimpeded pores. This quality renders them exceptionally well-suited for humidity sensing applications due to their augmented surface area, which offers an increased scope for interaction.

2. Experimental methodology

2.1. Materials required

In this work, the precursors utilized for the synthesis of WO_3/COK-12 nanostructures include sodium silicate solution (extra pure, Merck; Apurva Biotech, Karnal, India), Pluronic P123 (M_w = 5800 g mol^{-1}, Sigma Aldrich; Apurva Biotech, Karnal, India), anhydrous citric acid (AR, 99.5%, Sigma Aldrich; Apurva Biotech, Karnal, India), trisodium citrate dihydrate (Sigma Aldrich; Apurva Biotech, Karnal, India) and sodium tungstate dihydrate ($Na_2WO_4{\cdot}2H_2O$, Sigma Aldrich; Apurva Biotech, Karnal, India). All the investigations were carried out using double distilled water purchased from Organo Biotech Laboratories Pvt. Ltd, New Delhi, India. All the reagents were of analytical grade and used as received without further purification.

2.2. Preparation of samples

2.2.1. COK-12 synthesis. Synthesis of COK-12 followed a previously documented procedure[18,19] and was conducted at room temperature. In a typical procedure, 4.0 g of P123 was dissolved in 107.5 mL of distilled water. Once P123 had completely dissolved, 3.36 g of anhydrous citric acid and 2.82 g of trisodium citrate dihydrate were introduced to maintain the pH at 5. This mixture was continuously stirred for a duration of 24 h. Separately, a solution was prepared, comprising 10.4 g of sodium silicate dissolved in 30 mL of water, which was then added to the buffered solution. Solid particles formed immediately. The mixture was stirred for 5 minutes and then left to settle for 24 h without stirring. An additional step was carried out in which the mixture was poured into a stainless-steel closed chamber and was subjected to hydrothermal treatment at 90 °C for 24 h. After cooling down the steel chamber, the white material was separated from the mixture using centrifugation and purified by washing 5 times with distilled water. The obtained product was then dried

at 80 °C overnight. The dry material was heated in air at 550 °C with a gradual increase in temperature of 1 °C per minute and held for 8 h. This process removed the organic material completely. The final product was then stored in glass vials.

2.2.2. WO_3/COK-12 Synthesis. The same synthesis route was employed to produce nanostructures of COK-12 doped with tungsten. To create WO_3/COK-12 nanostructures, the measured amount of sodium tungstate dihydrate salt was incorporated into the P123 buffer solution prior to introducing the sodium silicate solution. The mixture was consistently stirred for a continuous duration of 3 h to ensure the even distribution of tungsten particles throughout. Subsequently, the necessary volume of sodium silicate solution was introduced gradually, and the resulting mixture was stirred for 5 minutes and then it was allowed to stand for 24 h. After that the same steps were followed as mentioned above to obtain the final product.

2.3. Characterization

The characterization of mesoporous COK-12 and its composites is a crucial step in evaluating its potential applications. Various techniques are employed to assess the material's properties, such as X-ray diffraction (XRD) to determine the crystal structure and phase composition with a range of 10° to 80° encapsulating a scan rate of 0.05. Scanning electron microscopy (SEM) provides insights into the surface morphology and film uniformity. Energy-dispersive X-ray spectroscopy (EDX) aids in analyzing elemental composition and verifying the presence of tungsten dopants. Small-angle X-ray scattering (SAXS) patterns were obtained at lower angles (0.9°–2.5°) utilizing a Primux 100 microfocus Cu X-ray source. High-Resolution transmission electron microscopy (HRTEM) images were acquired using a TECNAI microscope at 200 kV, after dispersing samples in absolute ethanol and depositing them on copper-coated TEM grids. Surface area analysis employed the Brunauer Emmett Teller (BET) method with N_2 adsorption–desorption measurements conducted at 77 K using ANTON PAR physisorption. A saturated vapor pressure of 99.3 kPa aided in determining the sample surface area *via* adsorption data. Pore characteristics were determined by the BJH method, assessing pore size and volume based on nitrogen adsorption following overnight vacuum degassing at 200 °C.

2.4. Development and evaluation of the humidity sensor

The responsiveness of both COK-12 and the hybrid nanostructures incorporating tungsten was investigated across a broad spectrum of humidity levels, encompassing the range from 11% to 98% relative humidity (RH) prevalent in the environment. To facilitate this examination, a mixture of the material was meticulously blended with ethanol and evenly deposited onto Ag–Pd interdigitated electrodes through a 10 μL pipette. To emulate various humidity levels encountered in real-world settings, a precisely controlled arrangement was adopted, involving sealed containers containing saturated salt solutions. For humidity levels corresponding to 11%, 33%, 54%, 75%, 84%, and 98% RH, distinct salt solutions were employed, namely lithium chloride (LiCl), magnesium chloride hexahydrate ($MgCl_2{\cdot}6H_2O$), magnesium nitrate tetrahydrate ($Mg(NO_3)_2{\cdot}4H_2O$), sodium chloride (NaCl), potassium chloride (KCl), and potassium sulfate, respectively. These solutions were consistently held at an ambient room temperature of 25 °C. The experimental arrangement employed for humidity sensing is elucidated in Fig. 1(a). In order to capture any shifts in resistance arising from the adsorption of H_2O molecules, an electrode with a coating of the testing material was placed in direct contact with the containers spanning various humidity levels. Throughout this procedure, a consistent source voltage was upheld *via* employment of a source meter. The subsequent resistance exhibited by the sensor was gauged in accordance with Ohm's law, thereby enabling the exploration of its direct correlation with altering humidity conditions. The ensuing fluctuations in resistance arising from shifts in humidity levels were meticulously recorded and subsequently subjected to comprehensive analysis. The sensor's operational effectiveness

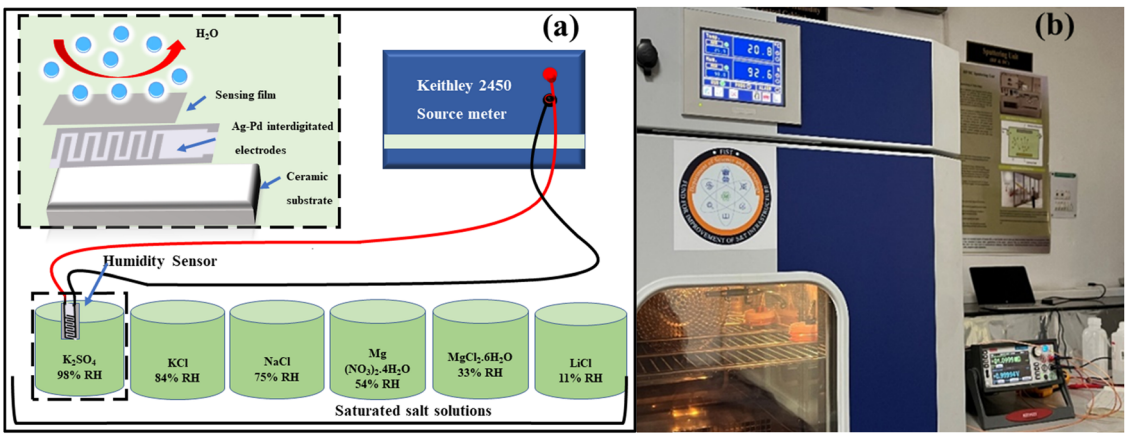

Fig. 1 (a) An illustration depicting the arrangement of the humidity-sensing setup, which includes various saturated salt solutions with distinct humidity levels, as well as the source meter; (b) cabinet for controlling temperature and humidity to maintain precise and stable temperature and humidity conditions.

was methodically assessed across a range of temperatures within the controlled environment displayed in Fig. 1(b).

3. Results and analysis

3.1. Small-angle X-ray scattering (SAXS)

The arrangement of hexagonal structures within calcined COK-12 materials was investigated through SAXS. Fig. 2 shows the SAXS patterns of both pure COK-12 and WO_3-infused COK-12 nanostructures. The observed SAXS patterns confirm the enduring preservation of the mesoporous structural integrity in both pure COK-12 and WO_3/COK-12 nanostructures. This is distinctly evident through the identification of characteristic diffraction peaks corresponding to the (100) and (110) reflection planes, which directly signify the presence of a consistent 2D hexagonal pore arrangement (space group *p6mm*) in the mesoporous structure.[19,20] The *p6mm* structure signifies a symmetrical arrangement of pores with six-fold rotational symmetry, forming a closely packed hexagonal lattice. This arrangement grants the material its unique and ordered architecture, which is crucial for its performance in humidity-sensing applications. The intensity of the (100) reflection goes on decreasing and the (110) reflection almost diminishes as tungsten loading increases. This phenomenon may stem from the partial reduction in structural regularity or the diminished differentiation between pore channels and walls that occurs as metal particles are introduced into the mesoporous silica's pore channels.

3.2. Wide angle X-ray diffraction (WAXRD)

Fig. 3 illustrates the wide-angle XRD patterns encompassing the range of 10° to 80° for both pure COK-12 and the synthesized hybrid WO_3/COK-12 nanostructures. Notably, at 2θ = 22°, a distinct hump becomes apparent, characteristic of the amorphous nature of mesoporous COK-12.[20] The associated peaks related to dopant particles were unnoticeable at lower WO_3 dopant concentrations, confirming the preservation of the mesoporous structure featuring its inherent amorphous planar walls.

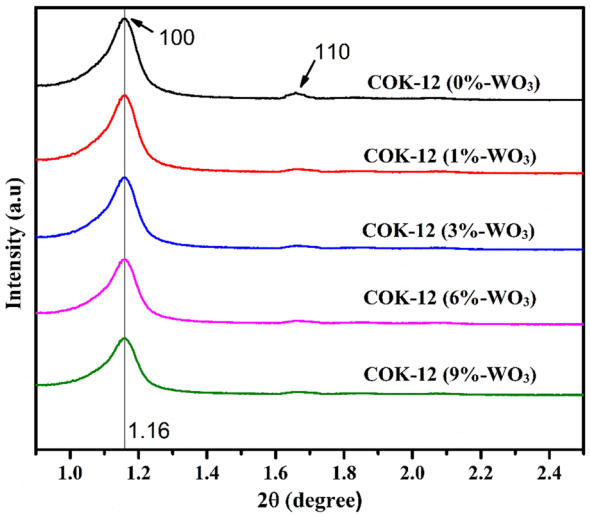

Fig. 2 Scattering patterns obtained through SAXS providing structural information for COK-12 and WO_3/COK-12 nanostructures.

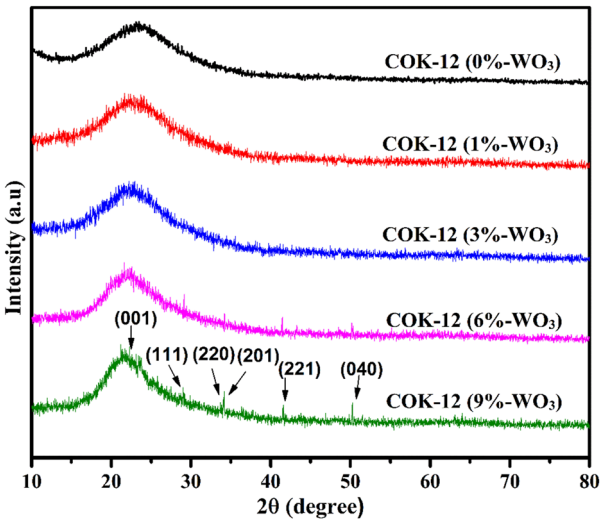

Fig. 3 WAXRD profiles revealing the crystalline structure of COK-12 and WO_3/COK-12 nanostructures.

Furthermore, with an increase in the WO_3 content within COK-12, multiple diffraction peaks arise at 2θ values of 22.61°, 29.04°, 33.71°, 34.16°, 41.57° and 50.37° without destroying the structural ordering. These align with lattice planes (001), (111), (220), (201), (221) and (040), respectively, corresponding to the distinct planes of WO_3 (JCPDS 20–1324).[21,22] It can be seen that the amorphous peak at 22° is getting somewhat narrower, which can be attributed to the crystalline phase introduced by the presence of WO_3 in the material. The associated diffraction peaks are of low intensity due to the high dispersion of tungsten on 2D hexagonal COK-12 support.

3.3. Field-emission scanning electron microscopy with energy dispersive X-ray spectroscopy (FESEM-EDX)

FESEM images of pure COK-12 are displayed in Fig. 4(a) and (b), revealing a connected granule-type morphology. The FESEM image with 1% tungsten content in the material also showcases this morphology as depicted in Fig. 4(c). Moving to the WO_3/COK-12 nanostructures with a more content of tungsten (Fig. 4(d)–(f)), it's evident that W particles are distributed both on the surface and within the pore network. This uniform dispersion of active components within the sensing material brings significant benefits, contributing to the achievement of optimal humidity-sensing outcomes.[23,24]

EDX analysis was conducted to verify the composition of WO_3/COK-12. The EDX spectra of pure COK-12 and the elemental compositions within its structure are depicted in Fig. 5(a). Notably, the presence of solely Si and O peaks suggests the absence of impurities in the prepared COK-12. In the case of the 6%-WO_3/COK-12 nanostructure, the emergence of tungsten peaks, alongside Si and O, as presented in Fig. 5(b) underlines the successful integration of tungsten into the COK-12 framework.

The elemental mapping images in Fig. 5(c–f) further reinforce these findings by revealing the uniform distribution of all elements within the synthesized material's framework.

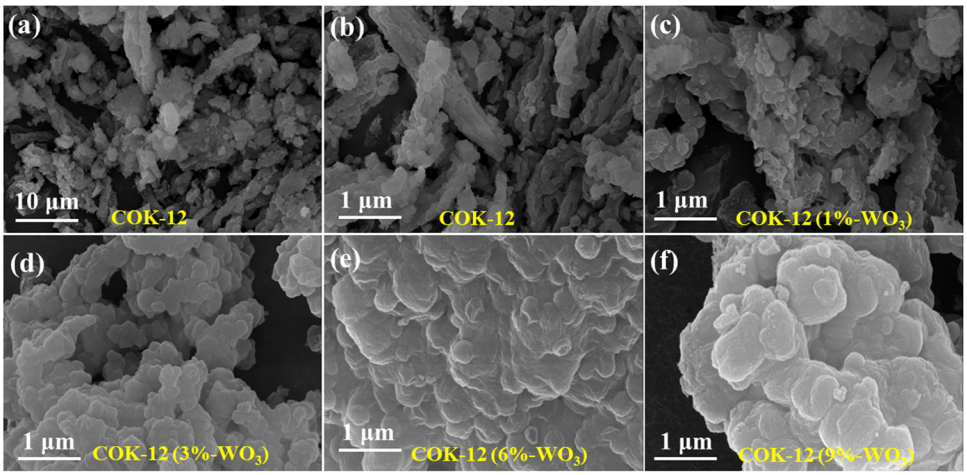

Fig. 4 FESEM recorded micrographs illustrating a granule-type morphological structure: (a) and (b) COK-12 and (c)–(f) WO_3/COK-12 nanostructures.

3.4 High-resolution transmission electron microscopy (HRTEM)

HRTEM images captured distinct features of the materials. In Fig. 6(a) and (b), the HRTEM images of pure COK-12 showcase an ordering of consistent pore channels, resembling a 2D hexagonal honeycomb array, with dimensions measuring around 20 nm and 50 nm. Moving to the HRTEM images of 6%-WO_3/COK-12 in Fig. 6(c) and (d), they reveal the presence of the tungsten nanoparticles situated within these pore channels.[25,26] The average size of these particles was determined to be approximately 5.01 nm as shown in the histogram in Fig. 7. Importantly, in the 6%-WO_3/COK-12 sample, the dissipation of tungsten particles across the mesoporous pathways within the support material is noteworthy. This substantiates the retention of the mesoporous structure even following tungsten accumulation.

3.5. Brunauer–Emmett–Teller (BET)

The adsorption–desorption isotherm curve, typically analyzed using the BET (Brunauer–Emmett–Teller) model, elucidates surface area and porosity characteristics of materials, aiding in understanding gas adsorption phenomena. Adsorption demonstrates the formation of a monolayer as gas pressure increases, followed by multilayer adsorption. Desorption shows hysteresis as gas is released due to higher desorption energy,

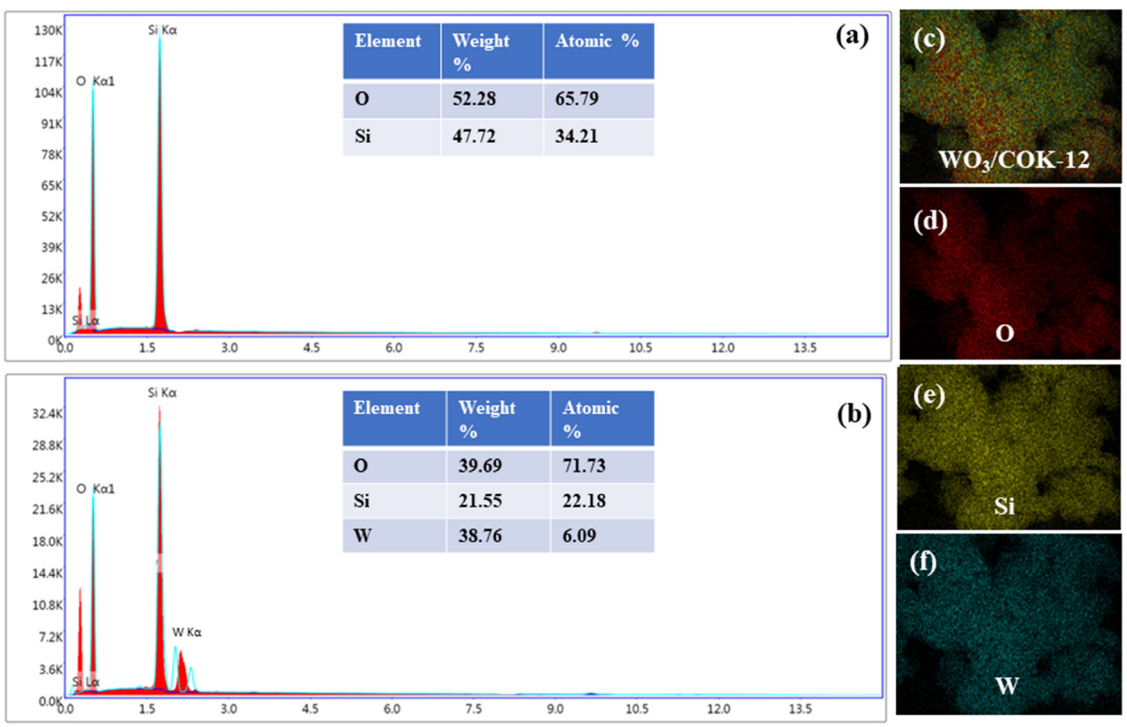

Fig. 5 EDX analysis describing the elemental composition: (a) COK-12 and (b) 6%-WO_3/COK-12 and (c)–(f) EDX elemental mapping.

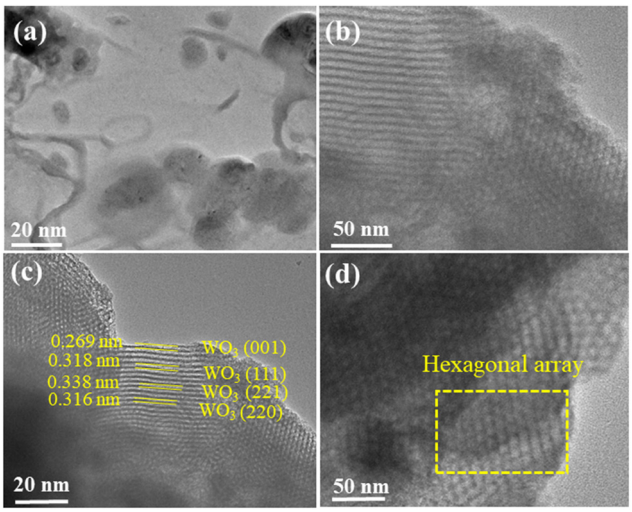

Fig. 6 HRTEM micrographs illustrating uniform pore channels: (a) and (b) COK-12 and (c) and (d) 6%-WO_3/COK-12 at 20 and 50 nm, respectively.

aiding in pore size distribution analysis. The N_2 adsorption–desorption isotherms in Fig. 8(a) illustrate the behavior of pure COK-12 and tungsten-loaded COK-12 nanostructures. Both material types show a type IV isotherm characterized by an H1-type hysteresis loop, indicative of ordered mesoporous structures featuring hexagonal pores with a well-organized *p6mm* geometry.[27,28] This confirms the sustained integrity of COK-12's ordered mesoporous framework after incorporating tungsten. The resulting material demonstrates a significantly high specific surface area of 864 m^2 g^{-1}. However, an observable trend emerges: as tungsten content increases, there is a gradual reduction in both surface area and pore size across all samples. This decline in BET-specific surface area suggests incomplete pore blockage due to the presence of tungsten within the pores, resulting in decreased mean pore diameter in WO_3/COK-12 samples. Pore size distribution curves (Fig. 8(b)) further support this trend, depicting a consistent decrease in average pore size with increasing tungsten loading in the mesostructure framework.

Table 1 presents a concise overview of the pore size, BET specific surface area, and pore volume metrics for COK-12 specimens. These characteristics bear significance in grasping the materials' porous structure and surface attributes, influencing their aptitude for adsorption and diffusion processes. The decrease in surface area can be attributed to tungsten's elevated atomic mass relative to silicon. This disparity introduces extra tungsten components that occupy certain internal surfaces, thereby contributing, to a certain degree, to the reduction in the effective surface area.

3.6. Humidity-sensing properties

To investigate the response of the prepared nanostructures across a wide range of humidity levels, changes in their resistance were compared and shown in Fig. 9(a). At a humidity level of 11% RH, all samples consistently display notably high resistance values exceeding 10^6 MΩ. As the relative humidity (RH) values increase, a systematic reduction in resistance is observed. Nevertheless, the reduction in resistance is comparably moderate when considering the pure mesoporous COK-12. On the other hand, the introduction of tungsten into the COK-12 structures leads to an enhanced response to humidity. The presence of tungsten leads to a noticeable alteration in resistance, particularly evident in the 6%-WO_3/COK-12 sample. This particular specimen showcases a remarkable alteration in resistance that covers an expansive span of about 4.3 orders of magnitude, covering the entire range of humidity values (11–98%).

With a gradual rise in humidity levels, water molecules undergo adsorption, forming a continuous layer on the nanostructure's surface. Consequently, the conduction of protons leads to a decrease in resistance. As humidity levels increase further, more water molecules are adsorbed, thickening the water layer. This process enables the splitting of the water molecules and allows the movement of hydronium ions through an easy path *i.e.*, the adsorbed layer. A detailed explanation of this response mechanism can be found in Section 3.7. In contrast, the 9 wt% WO_3 loaded COK-12 exhibits 4.3 orders of an on-scale resistance variation. Notably, higher amounts of W incorporations lead to a diminishing response, likely due to the potential blockage of pores within the matrix. This blockage hinders the flow of H_3O^+ ions across COK-12's mesoporous channels.

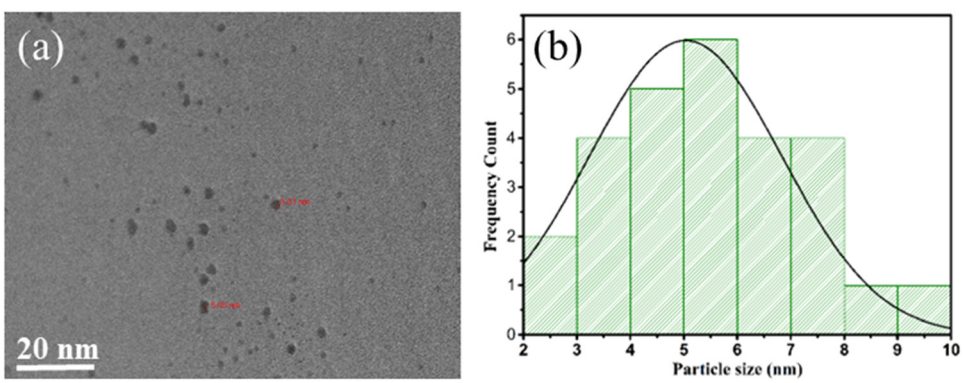

Fig. 7 (a) HRTEM image; (b) histogram for the particle size distribution of 6%-WO_3/COK-12.

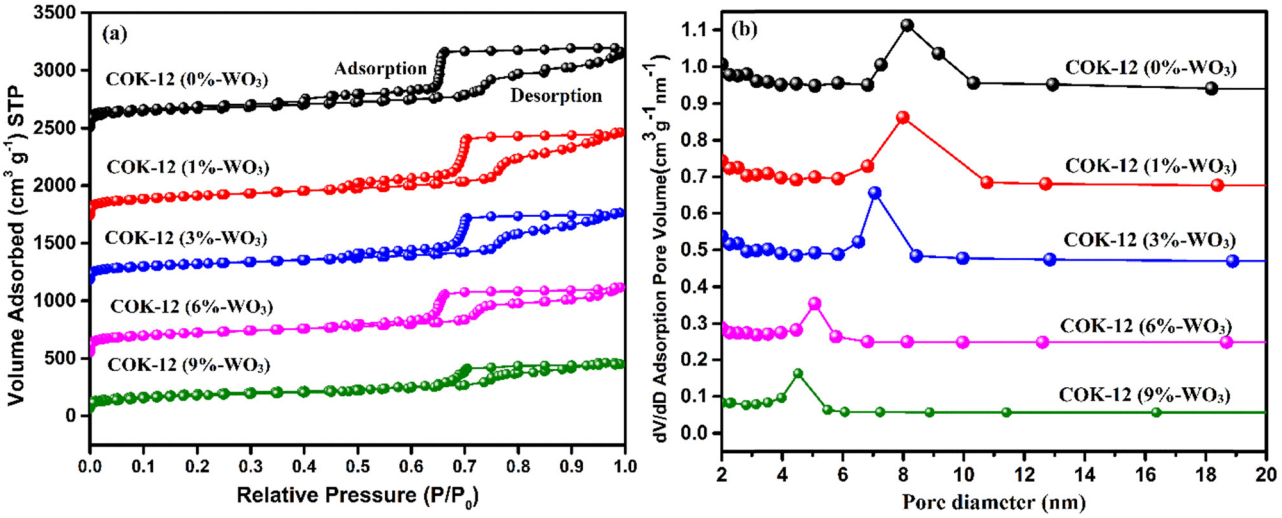

Fig. 8 (a) Nitrogen hysteresis isotherms; (b) pore-size distribution for synthesized COK-12 and WO_3/COK-12 nanostructures displaying a decrease in the pore size with an increase in the tungsten content.

Table 1 Structural characteristics of COK-12 and WO_3/COK-12 nanostructures

Sample	Pore diameter D_P (nm)	Specific surface area S_{BET} (m^2 g^{-1})	Pore volume V_P (cm^3 g^{-1})
COK-12	8.07	864.28	1.11
(1%-WO_3)/COK-12	7.98	853.62	1.06
(3%-WO_3)/COK-12	7.04	840.73	0.93
(6%-WO_3)/COK-12	5.10	821.79	0.87
(9%-WO_3)/COK-12	4.46	799.82	0.79

The response and recovery time of a humidity sensor are important parameters to evaluate its performance. Response time, in the context of adsorption, is the duration it takes for a sensor to reach 90% of its total response. On the other hand, recovery time, which applies to desorption, is the time it takes for the sensor to return to 90% of its initial state after being exposed to the sensing material. Fig. 10(a) depicts the experimental sensor response and recovery across different humidity levels. The sensor containing 6%-WO_3/COK-12 demonstrated a response of roughly 12 s and a recovery time of 11 s which was also found to be quite consistent with response time. To comprehend the temporal gap and consistency of the sample *i.e.* adsorption and desorption phases, a hysteresis loop was formulated, depicted in Fig. 10(b). Within this hysteresis curve, the black spherical line corresponds to adsorption (humidification) measurements ranging from 11% RH to 98% RH, whereas the red spherical line signifies desorption (dehumidification) evaluation. It is worth highlighting that 6%-WO_3/COK-12 displayed minimal hysteresis.

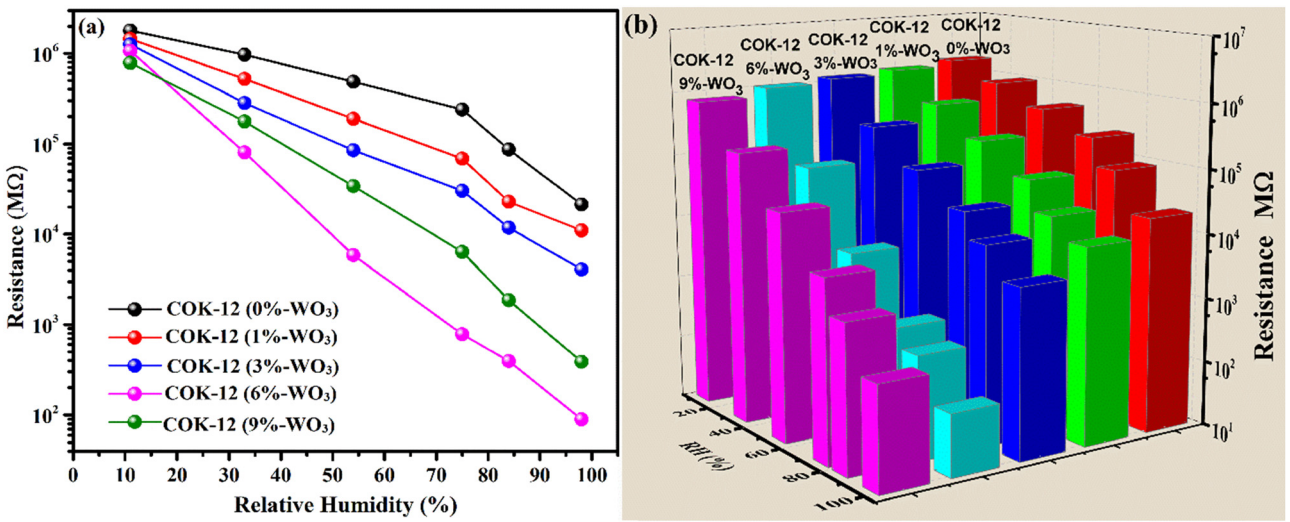

Fig. 9 (a) Humidity response curves; (b) 3-D bar chart, illustrating resistance reduction with increasing %RH for COK-12 and WO_3/COK-12 nanostructures.

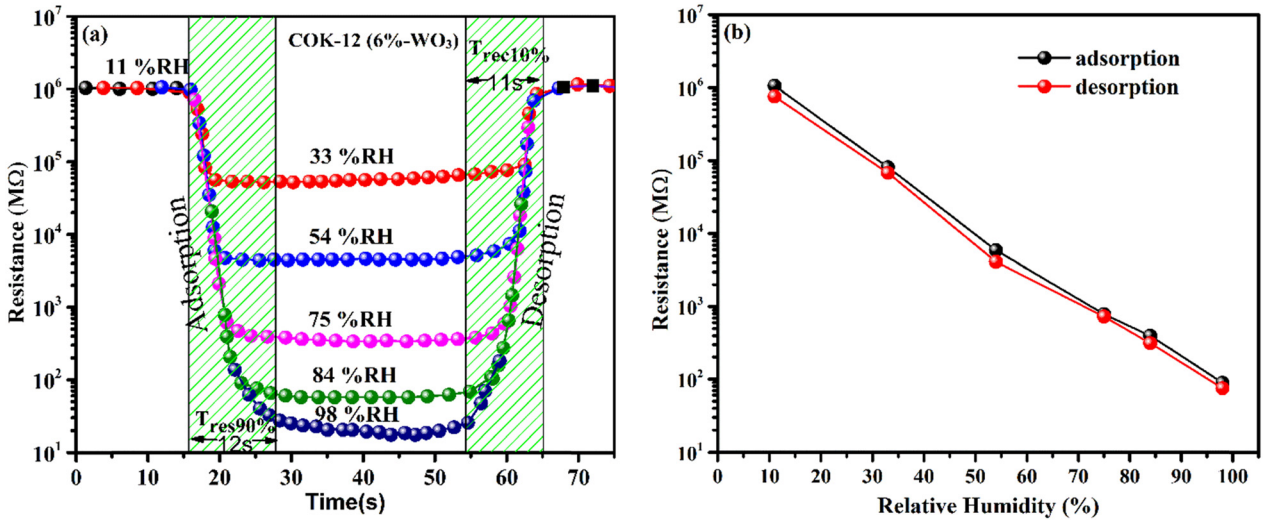

Fig. 10 (a) Response/recovery curve across diverse humidity levels for the 6%-WO3/COK-12 configuration; (b) Hysteresis curve displaying the lag between the adsorption and desorption process of the sensor.

Table 2 Comparing humidity-sensing traits of different materials as documented in the existing literature

Sr. No.	Material	Hysteresis	RH Range	Response time(s)	Recovery time(s)	Ref.
1	$FeWO_4$-WO_3 composite	—	5–98%	45	100	29
2	$HgWO_4$-WO_3 composite	—	5–98%	30	90	30
3	NaCl/KIT-6	—	11–95%	47	150	31
4	WO_3 nanosheets	—	10–90%	25	15	32
5	NGO-WO_3 composite	—	5–98%	24	53	33
6	Co-doped SnO_2/rGO	—	11–97%	50	100	34
7	Cobalt doped MoS_2	Negligible	10–90%	88	85	35
8	Gd-doped $CoCr_2O_4$	—	0–90%	150	—	36
9	ZnO/SnO_2	—	40–90%	411	98	37
10	Co-SBA-16	Negligible	11–98%	43	25	38
11	Poly(o-anisidine)/WO_3	6%	11–95%	82	81	39
12	Ag/WO_3	3%	11–95%	117	411	40
13	WO_3/KIT-6	Negligible	11–98%	21	24	41
14	WO_3/SnO_2	3%	11–95%	117	411	42
15	WO_3/SBA-15	2.6%	11–98%	18	25	43
16	WO_3/COK-12	Negligible	11–98%	12	11	This work

The efficiency of humidity sensors significantly depends on the attributes of the sensing active components. To comprehensively evaluate the efficacy of the synthesized WO_3/COK-12 nanostructures as humidity-sensing compatible materials, we have correlated their moisture detection attributes with those of diverse sensing efficient materials previously discussed in the research. In comparison with Table 2, we have consolidated the response parameters of such materials documented in earlier studies, encompassing the specified range of ambient relative humidity (RH) limits. This thorough juxtaposition unequivocally demonstrates that the WO_3/COK-12 nanostructures manifest exceptional response and recovery times across an extensive spectrum of RH values, surpassing a multitude of alternative materials. This encompasses various kinds of materials in literature such as composites of organic compounds or oxides based on mesoporous silica, thereby accentuating their superior performance.

Furthermore, the durability test of the sensor was traced by examining its relative humidity response over 32 days at four-day intervals, as shown in Fig. 11(a). Remarkably, the resistance exhibited almost no shift, confirming the exceptional stability and dependability of the sensor. The sensor's sensitivity (S) was calculated using the formula, $S = \frac{R(l) - R(h)}{\mathrm{RH}(l) - \mathrm{RH}(h)} \times 100$, where, $R(l)$ signifies the resistance at lower relative humidity (RH), while $R(h)$ denotes the resistance at higher RH levels. RH(l) and RH(h) correspond to lower and higher levels of humidity, respectively.[38] WO_3/COK sensor's sensitivity is visually presented in Fig. 11(b) within the 11–98% RH range. Notably, it demonstrates a linear increase as the RH percentage rises. These results underscore the remarkable sensing prowess of the WO_3/COK-12 sensor throughout the entire spectrum of relative humidity conditions.

The sensor's performance was systematically evaluated over a temperature range, as depicted in Fig. 11(c). A prominent rise in the response of the sensor was observed at the initial range of temperature from 20 °C to 80 °C. This behavior can be

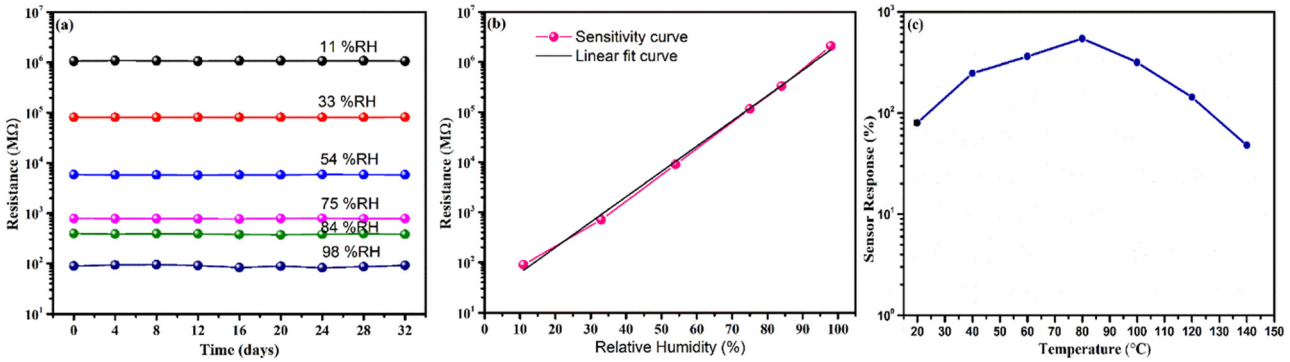

Fig. 11 (a) Stability of the sensor depicted through the response curve at various relative humidity levels over 24 days; (b) evaluating sensor's relative sensitivity within the (11–98) %RH range; (c) influence of temperature variation towards the sensor's response.

assigned to the heightened adsorption of hydronium ions onto the sensor's surface. This phenomenon arises from the increased kinetic energy of water molecules at elevated temperatures, facilitating their diffusion and interplay with the sensor.[44] Nevertheless, past a specific threshold, a reduction in sensor reactivity became apparent at elevated temperatures.[45,46] This decreases additional water molecules, resulting in an overall reduction in response. In contrast, lower temperatures can slow down response time due to the sluggish movement of water molecules.

3.7. Grotthuss mechanism

The phenomenon responsible for the transportation of hydronium ions (H_3O^+) under these ambient conditions of relative humidity was explained using the Grotthuss mechanism. This mechanism relies on the rapid movement of protons through a network of hydrogen bonds formed between water molecules. When water, a polar molecule, dissociates, it generates H^+ and OH^- ions, which interact with the first chemisorption layer involved in this mechanism. The hydroxyl ion can readily bond with[47–49] another water molecule, forming a new hydronium ion, which perpetuates the process, resulting in a conductive nature of the material. The WO_3 nanoparticles serve as adsorption sites for water molecules, which increases the number of water molecules that can be absorbed by the COK-12 material. The water molecules then undergo proton hopping through the Grotthuss mechanism, as described in Fig. 12, which generates an electrical signal that is proportional to the relative humidity of the surrounding environment.

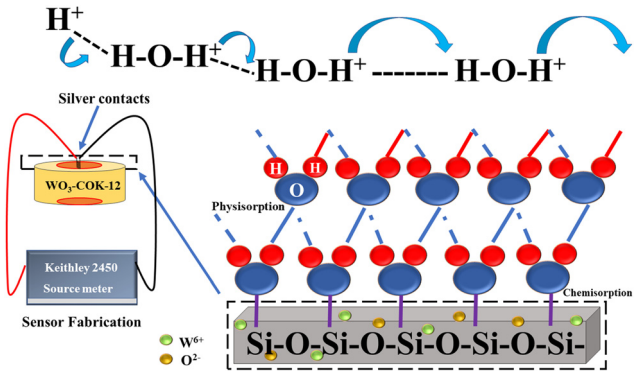

Fig. 12 Illustration of the Grotthuss chain mechanism in WO_3/COK-12 showcasing the proton-conducting process within the sensing material.

At higher relative humidity (R.H.) concentrations, the resistance value of the material experiences a substantial decrease compared to lower R.H. levels.[50] This behavior can be attributed to the Grotthuss mechanism, which governs the transport of hydronium ions (H_3O^+) under the given ambient conditions of R.H. The Grotthuss mechanism relies on the rapid movement of protons through a network of hydrogen bonds formed between water molecules. This facilitates the formation of a chemisorption layer where the hydroxyl ion, resulting from water dissociation, can readily bond with another water molecule, leading to the creation of a new hydronium ion *via* a physisorption process.[51] Proton hopping through the interconnected water network, which is formed by the chain of hydrogen bonds within the channels of the material's mesostructure, enables the rapid diffusion of hydronium ions throughout the medium.

The reactions involved in the Grotthuss mechanism can be summarized as follows:

(a) $H_2O \rightarrow H^+ + OH^-$ (Chemical adsorption).

(b) $2H_2O \rightarrow H_3O^+ + OH^-$ (Physical adsorption).

(c) $H_3O^+ \rightarrow H_2O + H^+$.

Conclusions

Our research has achieved a significant milestone in the development of a humidity sensor by ingeniously incorporating tungsten oxide into the microchannels of the COK-12 matrix. Through thorough examinations, we have confirmed the uniform dispersion of tungsten particles within mesopores. The WO_3/COK-12 sensor demonstrates an impressive resistance variation of 4.3 orders of magnitude across a wide relative humidity range (11% to 98%). It exhibits rapid response and recovery times (12 s and 11 s, respectively) and maintains exceptional stability over 32 days, highlighting its reliability. Moreover, the sensor's acute sensitivity allows it to detect subtle humidity fluctuations with precision. Beyond humidity sensing, our hybrid nanostructure opens the door to diverse applications,

including utilizing visible light for drug release and advancing water-splitting processes. This pioneering work paves the way for innovative and advanced scientific endeavors.

Author contributions

B. R. has significantly contributed to the conceptualization and design of the article, as well as the synthesis and analysis or interpretation of the article's data. M. S. G. and A. B. critically revised it to enhance its essential intellectual content. S. D. read and approved the final version of the manuscript and has agreed to be accountable for the accuracy and integrity of the work.

Conflicts of interest

There are no conflicts to declare.

Acknowledgements

Bhavna Rohilla and Aryan Boora, express gratitude to the University Grants Commission (UGC) for their support in funding the research through the Junior Research Fellowship (JRF) program, with reference number 221610112839 and 221610122664 respectively. The authors also extend their appreciation to the Department of Science and Technology (DST) in Delhi, India, for providing access to humidity sensing facilities as part of the Financial Assistance for Infrastructure Strengthening in Science and Technology (FIST) research grant, sanctioned under order number SR/FST/PS-1/2018/32.

References

1 A. Rivadeneyra, J. Fernández-Salmerón, M. Agudo, J. A. López-Villanueva, L. F. Capitan-Vallvey and A. J. Palma, Design and characterization of a low thermal drift capacitive humidity sensor by inkjet-printing, *Sens. Actuators, B*, 2014, **195**, 123–131, DOI: **10.1016/j.snb.2013.12.117**.

2 T. A. Blank, L. P. Eksperiandova and K. N. Belikov, Recent trends of ceramic humidity sensors development: A review, *Sens. Actuators, B*, 2016, **228**, 416–442, DOI: **10.1016/j.snb.2016.01.015**.

3 Ritu Malik, *et al.*, Functional gas sensing nanomaterials: A panoramic view, *Appl. Phys. Rev.*, 2020, **7**, 021301, DOI: **10.1063/1.5123479**.

4 S. Jakhar, S. Duhan and S. Nain, Novel one step hydrothermal synthesis of cubic Ia3d large pore 3D mesoporous In2O3/KIT-6 hybrid nanocomposite with humidity sensing applications, *J. Porous Mater.*, 2020, **27**(5), 1253–1263, DOI: **10.1007/s10934-020-00897**.

5 A. Kaushik, R. Kumar, S. K. Arya, M. Nair, B. D. Malhotra and S. Bhansali, Organic–inorganic hybrid nanocomposite-based gas sensors for environmental monitoring, *Chem. Rev.*, 2015, **115**(11), 4571–4606, DOI: **10.1021/cr400659h**.

6 D. J. Yu, W. Oum, A. Mirzaei, K. Y. Shin, E. B. Kim and H. M. Kim, … & Kim, H. W., Enhancement of xylene gas sensing by using Au core structures in regard to Au@ SnO2 core-shell nanocomposites, *Sens. Actuators, B*, 2023, **392**, 134018, DOI: **10.1016/j.snb.2023.134018**.

7 Q. Zhao, Z. Duan, Y. Wu, B. Liu, Z. Yuan, Y. Jiang and H. Tai, Facile primary battery-based humidity sensor for multifunctional application, *Sens. Actuators, B*, 2022, **370**, 132369, DOI: **10.1016/j.snb.2022.132369**.

8 M. Zhang, Z. Duan, B. Zhang, Z. Yuan, Q. Zhao, Y. Jiang and H. Tai, Electrochemical humidity sensor enabled self-powered wireless humidity detection system, *Nano Energy*, 2023, **115**, 108745, DOI: **10.1016/j.nanoen.2023.108745**.

9 Z. Duan, J. Li, Z. Yuan, Y. Jiang and H. Tai, Capacitive humidity sensor based on zirconium phosphate nanoplates film with wide sensing range and high response, *Sens. Actuators, B*, 2023, **394**, 134445, DOI: **10.1016/j.snb.2023.134445**.

10 Z. Cao, P. Du, A. Duan, R. Guo, Z. Zhao, H. Lei Zhang and Z. Chen, Synthesis of mesoporous materials SBA-16 with different morphologies and their application in dibenzothiophene hydrodesulfurization, *Chem. Eng. Sci.*, 2016, **155**, 141–152, DOI: **10.1016/j.ces.2016.08.001**.

11 Z. Duan, J. Li, Z. Yuan, Y. Jiang and H. Tai, Capacitive humidity sensor based on zirconium phosphate nanoplates film with wide sensing range and high response, *Sens. Actuators, B*, 2023, **394**, 134445, DOI: **10.1016/j.snb.2023.134445**.

12 Z. Duan, Q. Zhao, S. Wang, Q. Huang, Z. Yuan, Y. Zhang and H. Tai, Halloysite nanotubes: Natural, environmental-friendly and low-cost nanomaterials for high-performance humidity sensor, *Sens. Actuators, B*, 2020, **317**, 128204, DOI: **10.1016/j.snb.2020.128204**.

13 Y. I. N. G. Li and S. He, Study on MoO3/SBA-16 catalyzed transesterification to synthesize diphenyl carbonate, *Turk. J. Chem.*, 2022, **46**(6), 1930–1945.

14 M. Kondeboina, S. S. Enumula, V. R. B. Gurram, J. Yadagiri, D. R. Burri and S. R. R. Kamaraju, Mesoporous silica supported cobalt catalysts for gas phase hydrogenation of nitrobenzene: role of pore structure on stable catalytic performance, *New J. Chem.*, 2018, **42**(19), 15714–15725, DOI: **10.1039/C8NJ03211D**.

15 A. Kumar, G. Gupta, K. Bapna and D. D. Shivagan, Semiconductor-metal-oxide-based nano-composites for humidity sensing applications, *Mater. Res. Bull.*, 2023, **158**, 112053, DOI: **10.1016/j.materresbull.2022.112053**.

16 S. Jakhar, S. Duhan and S. Nain, Facile hydrothermal synthesis of mesoporous WO3/KIT-6 nanocomposite depicting great humidity sensitive properties, *Mater. Res. Innovations*, 2022, **26**(4), 203–213, DOI: **10.1080/14328917.2021.1940668**.

17 Z. Duan, Q. Zhao, S. Wang, Z. Yuan, Y. Zhang, X. Li and H. Tai, Novel application of attapulgite on high performance and low-cost humidity sensors, *Sens. Actuators, B*, 2020, **305**, 127534, DOI: **10.1016/j.snb.2019.127534**.

18 L. M. Henning, U. Simon, A. Gurlo, G. J. Smales and M. F. Bekheet, Grafting and stabilization of ordered mesoporous silica COK-12 with graphene oxide for enhanced removal of methylene blue, *RSC Adv.*, 2019, **9**(62), 36271–36284, DOI: **10.1039/C9RA05541J**.

19 L. H. Wee, M. Meledina, S. Turner, K. Custers, S. Kerkhofs, G. Van Tendeloo and J. A. Martens, Hematite iron oxide nanorod patterning inside COK-12 mesochannels as an efficient visible light photocatalyst, *J. Mater. Chem. A*, 2015, **3**(39), 19884–19891, DOI: **10.1039/C5TA05075H**.

20 A. L. Khan, S. P. Sree, J. A. Martens, M. T. Raza and I. F. Vankelecom, Mixed matrix membranes comprising of matrimid and mesoporous COK-12: Preparation and gas separation properties, *J. Membr. Sci.*, 2015, **495**, 471–478, DOI: **10.1016/j.memsci.2015.08.008**.

21 M. G. Colmenares, U. Simon, F. Schmidt, S. Dey, J. Schmidt, A. Thomas and A. Gurlo, Tailoring of ordered mesoporous silica COK-12: Room temperature synthesis of mesocellular foam and multilamellar vesicles, *Microporous Mesoporous Mater.*, 2018, **267**, 142–149, DOI: **10.1016/j.micromeso.2018.03.015**.

22 L. M. Henning, G. J. Smales, M. G. Colmenares, M. F. Bekheet, U. Simon and A. Gurlo, Synthesis and properties of COK-12 large-pore mesocellular silica foam, *Nano Select*, 2023, **4**(3), 202–212, DOI: **10.1002/nano.202200223**.

23 L. H. Wee, M. Meledina, S. Turner, K. Custers, S. Kerkhofs, S. P. Sree and J. A. Martens, Anatase TiO 2 nanoparticle coating on porous COK-12 platelets as highly active and reusable photocatalysts, *RSC Adv.*, 2016, **6**(52), 46678–46685, DOI: **10.1039/C6RA06141A**.

24 R. Pochamoni, A. Narani, M. Varkolu, M. U. R. A. L. I. Dhar Gudimella, S. S. Prasad Potharaju, D. R. Burri and S. R. Rao Kamaraju, Studies on ethylbenzene dehydrogenation with CO 2 as soft oxidant over Co 3 O 4/COK-12 catalysts, *J. Chem. Sci.*, 2015, **127**, 701–709, DOI: **10.1007/s12039-015-0826-x**.

25 M. Colmenares, *Ordered Mesoporous silica COK-12: Mesoscale tailoring, upscaling, continuous synthesis and application in the oxidative coupling of methane*, 2018, **vol. 1**, Universitätsverlag der TU Berlin, 9783798329881.

26 Y. Zhang, Y. Wu, Z. Duan, B. Liu, Q. Zhao, Z. Yuan and H. Tai, High performance humidity sensor based on 3D mesoporous Co3O4 hollow polyhedron for multifunctional applications, *Appl. Surf. Sci.*, 2022, **585**, 152698, DOI: **10.1016/j.apsusc.2022.152698**.

27 Z. Duan, Y. Jiang, Q. Zhao, S. Wang, Z. Yuan, Y. Zhang and H. Tai, Facile and low-cost fabrication of a humidity sensor using naturally available sepiolite nanofibers, *Nanotechnology*, 2020, **31**(35), 355501, DOI: **10.1088/1361-6528/ab932c**.

28 L. M. Henning, J. T. Müller, G. J. Smales, B. R. Pauw, J. Schmidt, M. F. Bekheet and U. Simon, Hierarchically porous and mechanically stable monoliths from ordered mesoporous silica and their water filtration potential, *Nanoscale Adv.*, 2022, **4**(18), 3892–3908, DOI: **10.1039/D2NA00368F**.

29 S. Poovaragan, R. Sundaram, C. M. Magdalane, K. Kaviyarasu and M. Maaza, Photocatalytic activity and humidity sensor studies of magnetically reusable FeWO4–WO3 composite nanoparticles, *J. Nanosci. Nanotechnol.*, 2019, **19**(2), 859–866, DOI: **10.1166/jnn.2019.15565**.

30 R. Renukadevi and R. Sundaram, Synthesis, characterization, humidity sensing, antibacterial, photocatalytic and kinetic studies of novel HgWO4–WO3 nanocomposites, *Mater. Today: Proc.*, 2019, **8**, 153–161, DOI: **10.1016/j.matpr.2019.02.094**.

31 X. He, W. Geng, B. Zhang, L. Jia, L. Duan and Q. Zhang, Ultrahigh humidity sensitivity of NaCl-added 3D mesoporous silica KIT-6 and its sensing mechanism, *RSC Adv.*, 2016, **6**(44), 38391–38398, DOI: **10.1039/C6RA03385G**.

32 M. Parthibavarman, M. Karthik and S. Prabhakaran, Facile and one step synthesis of WO3 nanorods and nanosheets as an efficient photocatalyst and humidity sensing material, *Vacuum*, 2018, **155**, 224–232, DOI: **10.1016/j.vacuum.2018.06.021**.

33 R. Ravichandran, S. D. Quine and M. V. Arularasu, Humidity Sensing Performance of Nitrogen Doped Reduced Graphene Oxide-WO3 Composite, *Bionanoscience*, 2023, 1–10, DOI: **10.1007/s12668-023-01193-z**.

34 A. I. Madbouly, M. Morsy and R. F. Alnahdi, Microwave-assisted synthesis of Co-doped SnO2/rGO for indoor humidity monitoring, *Ceram. Int.*, 2022, **48**(10), 13604–13614, DOI: **10.1016/j.ceramint.2022.01.240**.

35 R. K. Verma and R. K. Shukla, Hydrothermal synthesis of pristine and cobalt doped MoS2 nanosheets for comparative study and application in humidity sensing, *Mater. Today: Proc.*, 2023, DOI: **10.1016/j.matpr.2023.05.090**.

36 N. Ramprasad, F. Tudorache, G. V. Jagadeesha Gowda, A. El-Denglawey, K. S. Kantharaj, K. V. Arjuna Gowda and V. Jagadeesha Angadi, The effect of Gd as a dopant in crystal structure and on its electrical and humidity sensing behaviour of Co2+ Cr23+ O4 for possible application in sensors, *J. Mater. Sci.: Mater. Electron.*, 2022, **33**(17), 13584–13592, DOI: **10.1007/s10854-022-08293-8**.

37 N. D. Md Sin, M. H. Mamat, M. F. Malek and M. Rusop, Film-based humidity sensor with high sensitivity by ultrasonic-assisted solution growth method at different Zn: Sn precursor ratios, *Appl. Nanosci.*, 2014, **4**(7), 829–838, DOI: **10.1007/s13204-013-0262-5**.

38 Bhavna and S. Duhan, Modification of mesoporous SBA-16 with cobalt doping for outstanding humidity sensor at room temperature, *J. Porous Mater.*, 2023, 1–14, DOI: **10.1007/s10934-023-01499-z**.

39 D. Zhou, L. X. Pang, H. D. Xie, J. Guo, B. He, Z. M. Qi and C. A. Randall, Crystal structure and microwave dielectric properties of an ultralow-temperature-fired (AgBi) 0.5 WO4 ceramic, *Eur. J. Inorg. Chem.*, 2014, 296–301, DOI: **10.1002/ejic.201300789**.

40 N. K. Pandey, K. Tiwari, A. Roy, A. Mishra and A. Govindan, Ag-Loaded WO3 Ceramic Nanomaterials: Characterization and Moisture Sensing Studies, *Int. J. Appl. Ceram. Technol.*, 2013, **10**(1), 150–159, DOI: **10.1111/j.1744-7402.2011.02720.x**.

41 S. Jakhar, S. Duhan and S. Nain, Facile hydrothermal synthesis of mesoporous WO3/KIT-6 nanocomposite depicting great humidity sensitive properties, *Mater. Res. Innovations*, 2022, **26**(4), 203–213, DOI: **10.1080/14328917.2021.1940668**.

42 N. K. Pandey, V. Shakya and S. Mishra, Characterization and humidity sensing application of WO3-SnO2 nanocomposite, *IOSR, J. Appl. Phys.*, 2013, **4**(3), 10–17.

43 V. K. Tomer and S. Duhan, Highly sensitive and stable relative humidity sensors based on WO3 modified

mesoporous silica, *Appl. Phys. Lett.*, 2015, **106**, 6, DOI: 10.1063/1.4908116.

44 B. Yu, R. Shi, X. Chen, Y. Zhang, J. Hu and S. Khan, Gelatin-coated indomethacin drug-loaded SBA-16 silica-based composites: pH-responsive slow-release performance, *Inorg. Chem. Commun.*, 2023, **150**, 110469, DOI: 10.1016/j.inoche.2023.110469.

45 S. N. Azizi, S. Ghasemi, A. Samadi-Maybodi and M. Ranjbar-Azad, A new modified electrode based on Ag-doped mesoporous SBA-16 nanoparticles as non-enzymatic sensor for hydrogen peroxide, *Sens. Actuators, B*, 2015, **216**, 271–278, DOI: 10.1016/j.snb.2015.03.078.

46 R. Rajalakshmi, A. Rebekah, C. Viswanathan and N. Ponpandian, Evolution of intrinsic 1-3D WO3 nanostructures: Tailoring their phase structure and morphology for robust hydrogen evolution reaction, *Chem. Eng. J.*, 2022, **428**, 132013, DOI: 10.1016/j.cej.2021.132013.

47 V. K. Tomer and S. Duhan, A facile nanocasting synthesis of mesoporous Ag-doped SnO2 nanostructures with enhanced humidity sensing performance, *Sens. Actuators, B*, 2016, **223**, 750–760, DOI: 10.1016/j.snb.2015.09.139.

48 S. Nidhi Dahiya, A. Kumar, S. Duhan and M. S. Goyat, Single-pot hydrothermal derived TiO2/SBA-16 cubic mesoporous nanocomposite for humidity sensing, *J. Mater. Sci.*, 2022, **57**(5), 3441–3451, DOI: 10.1007/s10853-021-06822-0.

49 G. Jeevitha, S. Sivaselvam, S. Keerthana, D. Mangalaraj and N. Ponpandian, Highly effective and stable MWCNT/WO3 nanocatalyst for ammonia gas sensing, photodegradation of ciprofloxacin and peroxidase mimic activity, *Chemosphere*, 2022, **297**, 134023, DOI: 10.1016/j.chemosphere.2022.134023.

50 E. Poonia, P. K. Mishra, V. Kiran, J. Sangwan, R. Kumar, P. K. Rai and Y. K. Mishra, Aero-gel based CeO 2 nanoparticles: synthesis, structural properties and detailed humidity sensing response, *J. Mater. Chem. C*, 2019, **7**(18), 5477–5487, DOI: 10.1039/C9TC01081E.

51 E. Poonia, S. Duhan, K. Kumar, A. Kumar, S. Jakhar and V. K. Tomer, One pot hydrothermal synthesis of ordered mesoporous SnO 2/SBA-16 nanocomposites, *J. Porous Mater.*, 2019, **26**, 553–560, DOI: 10.1007/s10934-018-0651-y.